Direct Active and Reactive Power Regulation of DFIG Using Sliding-Mode Control Approach

Jiabing Hu, *Member, IEEE*, Heng Nian, *Member, IEEE*, Bin Hu, Yikang He, *Senior Member, IEEE*, and Z. Q. Zhu, *Fellow, IEEE*

***Abstract*—This paper presents a new direct active and reactive power control (DPC) of grid-connected doubly fed induction generator (DFIG)-based wind turbine systems. The proposed DPC strategy employs a nonlinear sliding-mode control scheme to directly calculate the required rotor control voltage so as to eliminate the instantaneous errors of active and reactive powers without involving any synchronous coordinate transformations. Thus, no extra current control loops are required, thereby simplifying the system design and enhancing the transient performance. Constant converter switching frequency is achieved by using space vector modulation, which eases the designs of the power converter and the ac harmonic filter. Simulation results on a 2-MW grid-connected DFIG system are provided and compared with those of classic voltage-oriented vector control (VC) and conventional lookup table (LUT) DPC. The proposed DPC provides enhanced transient performance similar to the LUT DPC and keeps the steady-state harmonic spectra at the same level as the VC strategy.**

***Index Terms*—Constant switching frequency, direct power control (DPC), doubly fed induction generators (DFIGs), sliding-mode control (SMC), wind power.**

NOMENCLATURE

$\boldsymbol{I}_s$, $\boldsymbol{I}_r$	Stator, rotor current vectors.
L_m	Mutual inductance.
L_s, L_r	Stator, rotor self-inductances.
$L_{\sigma s}$, $L_{\sigma r}$	Stator, rotor leakage inductances.
P_s, Q_s	Stator output active and reactive powers.
R_s, R_r	Stator, rotor resistances.
$\boldsymbol{U}_s$, $\boldsymbol{U}_r$	Stator, rotor voltage vectors.
θ_r	Rotor angle.
$\boldsymbol{\psi}_s$, $\boldsymbol{\psi}_r$	Stator, rotor flux linkage vectors.
ω_1, ω_r, ω_{slip}	Stator, rotor, and slip angular frequencies.
Subscripts	
α_s, β_s	Stationary $\alpha_s\beta_s$ axis.
α_r, β_r	Rotor $\alpha_r\beta_r$ axis.
s, r	Stator, rotor.
Superscripts	
s, r	Stator $\alpha_s\beta_s$, rotor $\alpha_r\beta_r$ reference frames.
$*$	Reference value for controller.
$\wedge$	Conjugate complex.

Manuscript received November 30, 2009; revised February 1, 2010 and March 8, 2010; accepted April 8, 2010. Date of publication June 14, 2010; date of current version November 19, 2010. This work was supported in part by the National Natural Science Foundation of China under Project 50907057. Paper no. TEC-00507-2009.

J. Hu and Z. Q. Zhu are with the Department of Electronic and Electrical Engineering, University of Sheffield, Sheffield S1 3JD, U.K. (e-mail: emec_zju@zju.edu.cn; emec_zju@hotmail.com; Z.Q.Zhu@sheffield.ac.uk).

H. Nian and Y. He are with the College of Electrical Engineering, Zhejiang University, Hangzhou 310027, China (e-mail: nianheng@zju.edu.cn; ykhe@zju.edu.cn).

B. Hu is with the Zhejiang Wind Power Development Corporation Ltd., Hangzhou, China (e-mail: raymond_hb@hotmail.com).

Digital Object Identifier 10.1109/TEC.2010.2048754

I. INTRODUCTION

DOUBLY fed induction generators (DFIGs) are extendedly used in modern wind power generation systems due to their variable speed operation, four-quadrant active and reactive power capability, low-converter cost, and reduced power losses compared with other solutions such as fixed speed induction generators or fully fed synchronous generators with fully sized converters.

Classic control of grid-connected DFIGs is usually based on either stator voltage oriented [1], [2] or stator-flux-oriented (SFO) [3], [4] vector control (VC). The scheme decouples the rotor current into active and reactive power components in the synchronous reference frame. Control of instantaneous stator active and reactive powers is then achieved by regulating the decoupled rotor currents, using proportional-integral (PI) controllers. One main drawback for this control scheme is that the performance highly relies on the tuning of the PI parameters and accurate machine parameters such as stator and rotor inductances and resistances. Thus, performance may degrade when actual machine parameters deviate from values used in the control system.

Considering discrete operation of voltage source inverters, direct torque control (DTC), as an alternative to the VC control for induction machines, was proposed in [5] and [6]. The DTC strategy provides direct torque regulation of the machine's torque, reduces the complexity of the VC strategy and minimizes the use of machine parameters. Initially, the basic DTC method directly controls the torque and flux by selecting voltage vectors from a predefined lookup table (LUT) based on the stator flux and torque information. One main problem [7] is that the converter switching frequency varies with operating conditions and torque/flux hysteresis controllers' bandwidth, which significantly complicates power circuit designs and results in obvious torque pulsations. Several efforts have been addressed to solve this problem by incorporating space vector modulation (SVM) technique, and meanwhile constant switching frequency was achieved [8]–[10]. In [8] and [9], inverter switching duty cycles were generated from torque and flux PI controllers, whereas in [10], they were calculated based on the instantaneous errors of torque and flux within each sampling period. In [11], the inverter's output voltage vectors were selected using the basic

DTC switching table while the duration time of every voltage vector was determined by the torque-ripple minimum strategy.

Recently, based on the principles of DTC, similar DTC or direct power control (DPC) strategies have also been developed to control DFIG systems [12]–[16]. In [12] and [13], the methods were based on an optimal switching table by using the information of estimated rotor flux and stator flux, respectively. However, like a basic DTC, LUT-based DPC has switching frequencies varying significantly with active and reactive power variations, the power controllers' hysteresis bandwidth as well as the machine operating velocity. As a result, the stator side ac filter preventing switching harmonics from injecting the connected grid needs to be designed to absorb broad-band harmonics, and the filter's efficiency is reduced with increased size and power losses. To solve this issue highlighted, in [14] and [15], the switching vectors were chosen based on a basic switching table and thereafter their duration times were optimized with the target of reducing pulsations in the torque or active power and flux or reactive power. Although a constant switching frequency was achieved, it required complicated online calculations and had oscillating problems when the generator operates around its synchronous speed. A simple constant switching frequency DPC strategy based on a predictive power model was developed in [16] and [17]. The method, however, was implemented in the synchronous reference frame, which necessitates the angular information of network voltage and the synchronous coordinate transformations.

Variable structure control or sliding-mode control (SMC) strategy is an effective and high-frequency switching control for nonlinear systems with uncertainties [18]–[20]. The design principles of SMC and its applications to electrical drive systems were initially proposed in [18]. It features simple implementation, disturbance rejection, strong robustness, and fast responses, but the controlled state may exhibit undesired chattering. Thus, a SMC-based DTC drive for induction machine was proposed in [19] and [20] with SFO and regulated. It is named linear and variable structure control, which employs a switching component and a linear one, and has dual behaviors.

Owing to the robustness with respect to external disturbance and unmodeled dynamics of wind turbines and generators, a few second-order SMC approaches have been introduced for renewable energy applications in terms of aerodynamic control [21], [22] and power converters control [23], [24]. In [21], a robust sliding-mode controller was proposed for the purpose of regulating power generation in variable-speed wind turbines. As a result, the stability in two operation regions, namely, low-speed and high-speed regions, is guaranteed, and the ideal feedback control solution despite mode uncertainties is imposed as well. The power reference is generated by a maximum power point tracking (MPPT) algorithm that searches for the peak power on the power–speed curve, but much of the time wind speed fluctuations force the turbine to operate off the peak of the MPPT curve. On the other hand, tight tracing of the MPPT curve would lead to significant mechanical stress and transfer aerodynamic fluctuations into the power system. This, as a consequence, will result in less energy capture. In order to improve the performance, a high-order SMC strategy was presented in [22] for variable-speed wind turbines, which combines

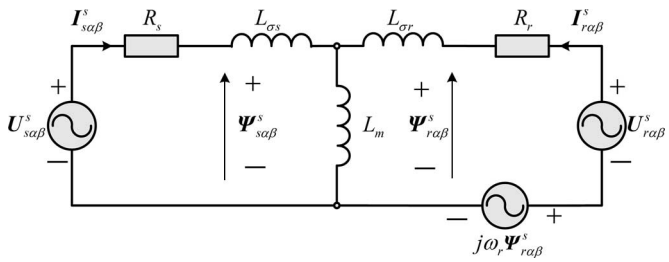

Fig. 1. Equivalent circuit of a DFIG in the stator stationary reference frame.

a second-order sliding-mode observer for the estimation of the aerodynamic torque together with a second-order sliding-mode controller for tracking the optimal torque. While for the rotor side converter of DFIG driven by marine current turbine [23] and wind turbine [24], respectively, second-order SMC schemes were proposed to regulate the d- and q-axis rotor currents or d-axis rotor current and electromagnetic torque with SFO in the synchronous reference frame. Apparently, similar to VC [1]–[4] and predictive DPC [13], [14] schemes, these converter's control strategies [23], [24] based on SMC approach, also require synchronous coordinate transformation associated with the angular information of stator flux. Besides, identical to classic VC scheme, additional outer control loop for active and reactive powers is required to generate the reference values of d- and q-axis rotor currents as well.

In order to tackle the drawback highlighted earlier, this paper presents a new direct active and reactive power regulation schemes for grid-connected DFIGs, using nonlinear SMC approach. The proposed SMC-based DPC is capable of simply regulating the instantaneous active and reactive powers without any rotor current control loops and synchronous coordinate transformations involved. The required rotor control voltage can be directly obtained in the stator stationary reference frame and SVM technique is employed to achieve constant switching frequency. As a result, enhanced transient performance similar to the conventional LUT DPC is obtained and steady-state stator and rotor current harmonic spectra are kept at the same level as the classic VC strategy due to the use of SVM module. The rest part of the paper is organized as follows. Section II gives dynamic behavior of grid-connected DFIG in the stationary reference frame and the associated instantaneous stator active and reactive power flows. With conventional LUT DPC briefly described, SMC-based DPC strategy is proposed, designed, and analyzed in Section III. Section IV presents the simulation results to demonstrate the performance of the proposed DPC strategy. Finally, the conclusions are made in Section V.

II. Dynamic Behavior of a DFIG in the Stator Stationary Reference Frame

The equivalent circuit of a DFIG represented in the stator stationary reference frame is shown in Fig. 1. As it is shown, in the stator stationary reference frame, the stator and rotor flux linkage vectors can be given as

$$\begin{aligned} \boldsymbol{\psi}^s_{s\alpha\beta} &= L_s \boldsymbol{I}^s_{s\alpha\beta} + L_m \boldsymbol{I}^s_{r\alpha\beta} \\ \boldsymbol{\psi}^s_{r\alpha\beta} &= L_m \boldsymbol{I}^s_{s\alpha\beta} + L_r \boldsymbol{I}^s_{r\alpha\beta}. \end{aligned} \tag{1}$$

According to (1), the rotor flux linkage vector can be expressed in terms of stator current and stator flux linkage vectors as

$$\boldsymbol{\psi}^s_{r\alpha\beta} = \sigma L_m \boldsymbol{I}^s_{s\alpha\beta} + \frac{L_r}{L_m}\boldsymbol{\psi}^s_{s\alpha\beta} \tag{2}$$

where $\sigma = 1 - L_s L_r / L_m^2$ is leakage factor.

From Fig. 1, the stator and rotor voltage vectors are given in the stator stationary reference frame as

$$\begin{aligned}\boldsymbol{U}^s_{s\alpha\beta} &= R_s \boldsymbol{I}^s_{s\alpha\beta} + \frac{d\boldsymbol{\psi}^s_{s\alpha\beta}}{dt}\\ \boldsymbol{U}^s_{r\alpha\beta} &= R_r \boldsymbol{I}^s_{r\alpha\beta} + \frac{d\boldsymbol{\psi}^s_{r\alpha\beta}}{dt} - j\omega_r \boldsymbol{\psi}^s_{r\alpha\beta}.\end{aligned} \tag{3}$$

Based on (2) and (3), the instantaneous variations of stator current can be expressed as

$$\begin{aligned}\frac{d\boldsymbol{I}^s_{s\alpha\beta}}{dt} = {} & \frac{1}{\sigma L_m}\left[\boldsymbol{U}^s_{r\alpha\beta} - R_r \boldsymbol{I}^s_{r\alpha\beta} - \frac{L_r}{L_m}\left(\boldsymbol{U}^s_{s\alpha\beta} - R_s \boldsymbol{I}^s_{s\alpha\beta}\right)\right]\\ & + \frac{j\omega_r}{\sigma L_m}\left(\sigma L_m \boldsymbol{I}^s_{s\alpha\beta} + \frac{L_r}{L_m}\boldsymbol{\psi}^s_{s\alpha\beta}\right).\end{aligned} \tag{4}$$

The instantaneous stator active and reactive power outputs from the DFIG to the network side can be calculated as

$$P_s + jQ_s = -1.5\boldsymbol{U}^s_{s\alpha\beta} \times \hat{\boldsymbol{I}}^s_{s\alpha\beta} \tag{5}$$

and

$$P_s = -1.5\left(u_{s\alpha} i_{s\alpha} + u_{s\beta} i_{s\beta}\right) \tag{6a}$$

$$Q_s = -1.5\left(u_{s\beta} i_{s\alpha} - u_{s\alpha} i_{s\beta}\right) \tag{6b}$$

where $P_s > 0$ and $P_s < 0$ mean that the DFIG operates as a generator and a motor, respectively, $Q_s > 0$ and $Q_s < 0$ denote that the DFIG exports capacitive and inductive reactive power to the grid, respectively.

Besides, the electromagnetic torque can be expressed using the following equation:

$$\begin{aligned}T_e &= \frac{3}{2}\frac{pL_m \operatorname{Im}(\boldsymbol{\psi}^s_{s\alpha\beta} \times \hat{\boldsymbol{\psi}}^s_{r\alpha\beta})}{(\sigma L_s L_r)}\\ &= \frac{3}{2}\frac{pL_m(\boldsymbol{\psi}_{s\beta}\boldsymbol{\psi}_{r\alpha} - \boldsymbol{\psi}_{s\alpha}\boldsymbol{\psi}_{r\beta})}{(\sigma L_s L_r)}\end{aligned} \tag{7}$$

where p is the number of pole pairs.

Consequently, the mechanoelectrical equation of a wind-turbine driven DFIG system is expressed as

$$\frac{J}{p}\frac{d\omega_r}{dt} = T_m - T_e \tag{8}$$

where J is inertia constant, T_e can be calculated from (7), T_m is the output torque of wind turbine and can be obtained from the optimum torque–speed curve between the cut-in wind speed and limited wind speed as [21], [22]

$$T_m = K_{\text{opt}}\left(\frac{\omega_r}{p}\right)^2 \tag{9}$$

where K_{opt} is the optimal torque constant of wind turbine.

Differentiating (6) results in instantaneous variations of stator active and reactive powers as

$$\frac{dP_s}{dt} = -\frac{3}{2}\left(u_{s\alpha}\frac{di_{s\alpha}}{dt} + i_{s\alpha}\frac{du_{s\alpha}}{dt} + u_{s\beta}\frac{di_{s\beta}}{dt} + i_{s\beta}\frac{du_{s\beta}}{dt}\right) \tag{10a}$$

$$\frac{dQ_s}{dt} = -\frac{3}{2}\left(u_{s\beta}\frac{di_{s\alpha}}{dt} + i_{s\alpha}\frac{du_{s\beta}}{dt} - u_{s\alpha}\frac{di_{s\beta}}{dt} - i_{s\beta}\frac{du_{s\alpha}}{dt}\right). \tag{10b}$$

As expressed in (10), the network voltage variation is required, considering an ideal network, namely,

$$\begin{aligned}u_{s\alpha} &= U_s \sin(\omega_1 t)\\ u_{s\beta} &= U_s \sin(\omega_1 t - \pi/2) = -U_s \cos(\omega_1 t).\end{aligned} \tag{11}$$

Thus, the instantaneous network voltage variation can be obtained as

$$\begin{aligned}\frac{du_{s\alpha}}{dt} &= \omega_1 U_s \cos(\omega_1 t) = -\omega_1 u_{s\beta}\\ \frac{du_{s\beta}}{dt} &= \omega_1 U_s \sin(\omega_1 t) = \omega_1 u_{s\alpha}.\end{aligned} \tag{12}$$

Based on (4), the instantaneous stator current variations can be expressed with respective α, β components as

$$\begin{aligned}\frac{di_{s\alpha}}{dt} = {} & \frac{1}{\sigma L_m}\left[u_{r\alpha} - R_r i_{r\alpha} - \frac{L_r}{L_m}\left(u_{s\alpha} - R_s i_{s\alpha}\right)\right]\\ & - \frac{\omega_r}{\sigma L_m}\left(\sigma L_m i_{s\beta} + \frac{L_r}{L_m}\boldsymbol{\psi}_{s\beta}\right)\\ \frac{di_{s\beta}}{dt} = {} & \frac{1}{\sigma L_m}\left[u_{r\beta} - R_r i_{r\beta} - \frac{L_r}{L_m}\left(u_{s\beta} - R_s i_{s\beta}\right)\right]\\ & + \frac{\omega_r}{\sigma L_m}\left(\sigma L_m i_{s\alpha} + \frac{L_r}{L_m}\boldsymbol{\psi}_{s\alpha}\right).\end{aligned} \tag{13}$$

Substituting (12) and (13) into (10) and arranging them in matrix form yield

$$\begin{aligned}\frac{d}{dt}\begin{bmatrix}P_s\\ Q_s\end{bmatrix} = {} & -\frac{3}{2}\frac{1}{\sigma L_m}\begin{bmatrix}u_{s\alpha} & u_{s\beta}\\ u_{s\beta} & -u_{s\alpha}\end{bmatrix}\begin{bmatrix}u_{r\alpha}\\ u_{r\beta}\end{bmatrix}\\ & - \frac{3}{2}\frac{\omega_r L_r}{\sigma L_m^2}\begin{bmatrix}u_{s\beta} & -u_{s\alpha}\\ -u_{s\alpha} & -u_{s\beta}\end{bmatrix}\begin{bmatrix}\boldsymbol{\psi}_{s\alpha}\\ \boldsymbol{\psi}_{s\beta}\end{bmatrix}\\ & - \frac{3}{2}\frac{R_r}{\sigma L_m}\begin{bmatrix}-u_{s\alpha} & -u_{s\beta}\\ -u_{s\beta} & u_{s\alpha}\end{bmatrix}\begin{bmatrix}i_{r\alpha}\\ i_{r\beta}\end{bmatrix}\\ & + \begin{bmatrix}\frac{L_r}{\sigma L_m^2}R_s & -\omega_{\text{slip}}\\ \omega_{\text{slip}} & \frac{L_r}{\sigma L_m^2}R_s\end{bmatrix}\begin{bmatrix}P_s\\ Q_s\end{bmatrix}\\ & + \frac{3}{2}\frac{L_r}{\sigma L_m^2}\begin{bmatrix}u_{s\alpha}^2 + u_{s\beta}^2\\ 0\end{bmatrix}.\end{aligned} \tag{14}$$

where $\omega_{\text{slip}} = \omega_1 - \omega_r$ is slip angular frequency.

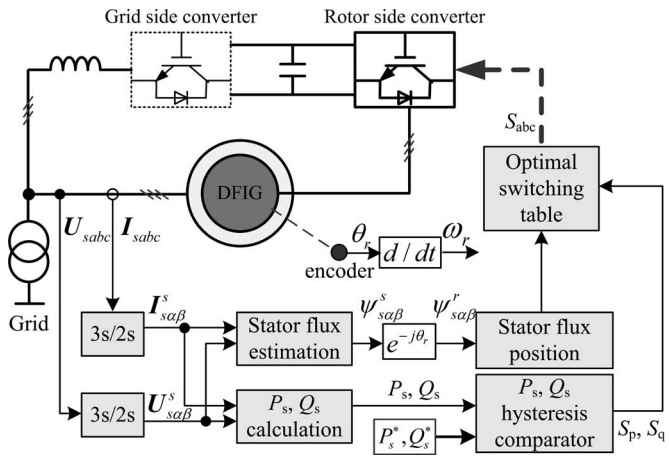

Fig. 2. Schematic diagram of conventional LUT DPC for a grid-connected DFIG system.

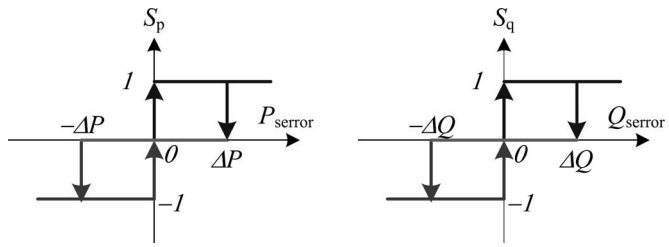

Fig. 3. Active and reactive power hysteresis comparators.

III. Proposed DPC Using SMC Approach

A. Conventional LUT DPC

According to the principle of the conventional DPC for a grid-connected DFIG, at each sampling instant an appropriate voltage vector is selected by the switching rule to restrict the instantaneous active and reactive powers within their required hysteresis bands, respectively. The scheme is illustrated in Fig. 2. The active and reactive power controllers are three level hysteresis comparators, as shown in Fig. 3. The comparators generate discrete signals S_p and S_q, as inputs to the switching table based on the active and reactive power errors. With the error signs from the hysteresis controllers and referring to the sector where the estimated stator flux is located, the switching rule directly produces the converter's switching signals S_{abc} from a predefined LUT. The DPC algorithm is accomplished in the rotor reference frame rotating at the angular speed of ω_r without involving any pulsewidth modulation (PWM) module, which gets the maximum dynamic performance available.

However, it has been highlighted that the conventional LUT DPC [13]for a grid-connected DFIG system is a hysteresis bang–bang control by applying single full voltage vector within each sampling period and hence results in high chattering in the active and reactive powers. Even worse, its main drawback is the resulting variable switching frequency, which is usually not bounded and depends mainly on the sampling time, LUT structure, load parameters, and operational state of the system. Thus, the LUT DPC generates a dispersed harmonic spectrum, making it pretty difficult to design the ac filter for grid-connected DFIG systems so as to avoid unexpected power system resonance.

A new DPC by combining SMC approach and SVM technique is proposed and described for grid-connected DFIGs in the following section. In such way, both high-transient responses and constant switching frequency are obtained.

B. Proposed DPC Based on SMC

The SMC strategy with variable control structure is based on the design of discontinuous control signal that drives the system operation states toward special manifolds in the state space [18]. These manifolds are chosen in a way that the control system will have the desired behavior as the states converge to them. In this paper, based on the conventional LUT DPC concept, an SMC scheme for directly regulating instantaneous stator active and reactive powers of grid-connected DFIGs is exploited.

1) Sliding Surface: The control objectives for DFIG systems are to track or slide along the predefined active and reactive power trajectories. Thus the sliding surface is set as

$$\boldsymbol{S} = [\, S_1 \quad S_2 \,]^T . \tag{15}$$

In order to maintain the enhanced transient response and minimize the steady-state error, the switching surfaces can be in the integral forms [25], [26], alternatively they can also be designed via back-stepping and nonlinear damping techniques [27]

$$\begin{aligned} S_1 &= e_P(t) + K_P \int_0^t e_P(\tau)d\tau + e_P(0) \\ S_2 &= e_Q(t) + K_Q \int_0^t e_Q(\tau)d\tau + e_Q(0) \end{aligned} \tag{16}$$

where $e_P(t) = P_s^* - P_s$ and $e_Q(t) = Q_s^* - Q_s$ are the respective errors between the references and the actual values of instantaneous stator active and reactive powers. K_P and K_Q are positive control gains. The manifolds $S_1 = 0$ and $S_2 = 0$ represent the precise tracking of DFIG's stator active and reactive powers. When the system states reach the sliding manifold and slide along the surface, then we have

$$S_1 = S_2 = \frac{dS_1}{dt} = \frac{dS_2}{dt} = 0. \tag{17}$$

According to (16) and (17), derivatives of S_1 and S_2 equal zero, which gives

$$\frac{de_P(t)}{dt} = -K_P e_P(t) \tag{18a}$$

$$\frac{de_Q(t)}{dt} = -K_Q e_Q(t). \tag{18b}$$

The aforementioned equations ensure the power errors converge to zero, where K_P and K_Q are positive constants and chosen for the required system transients. Since (16) equals null at the beginning, the active and reactive power systems will converge asymptotically to the origin with time constants of $1/K_P$ and $1/K_Q$, respectively. Then, the design task is aimed at accomplishing sliding mode in the manifolds $S_1 = 0$ and $S_2 = 0$ with discontinuous rotor voltage space vectors.

2) SMC Law: In an SMC design, as the name indicates, the task is to force the system state trajectory to the interaction of the switching surfaces mentioned earlier. In this paper, an SMC scheme is designed to generate the converter output voltage reference as an input to SVM module.

The motion projections of the system (10) and (14) on $\boldsymbol{S}$ subspace are derived, by differentiating $\boldsymbol{S}$ in (16), as

$$\begin{aligned}\frac{dS_1}{dt} &= \frac{de_P(t)}{dt} + K_P e_P(t) = -\frac{d}{dt}P_s + K_P\left(P_s^* - P_s\right)\\ \frac{dS_2}{dt} &= \frac{de_Q(t)}{dt} + K_Q e_Q(t) = -\frac{d}{dt}Q_s + K_Q\left(Q_s^* - Q_s\right).\end{aligned} \tag{19}$$

Substituting (14) into (19) leads to

$$\frac{d\boldsymbol{S}}{dt} = \boldsymbol{F} + \boldsymbol{D}\boldsymbol{U}_{r\alpha\beta}^{s} \tag{20}$$

where

$$\begin{aligned}\boldsymbol{F} &= [\,F_1 \quad F_2\,]^T \quad \boldsymbol{U}_{r\alpha\beta}^{s} = [\,u_{r\alpha} \quad u_{r\beta}\,]^T\\ \begin{bmatrix}F_1\\F_2\end{bmatrix} &= \frac{3\omega_r L_r}{2\sigma L_m^2}\begin{bmatrix}u_{s\beta} & -u_{s\alpha}\\ -u_{s\alpha} & -u_{s\beta}\end{bmatrix}\begin{bmatrix}\psi_{s\alpha}\\ \psi_{s\beta}\end{bmatrix}\\ &\quad + \frac{3R_r}{2\sigma L_m}\begin{bmatrix}-u_{s\alpha} & -u_{s\beta}\\ -u_{s\beta} & u_{s\alpha}\end{bmatrix}\begin{bmatrix}i_{r\alpha}\\ i_{r\beta}\end{bmatrix}\\ &\quad - \begin{bmatrix}\frac{L_r}{\sigma L_m^2}R_s & -\omega_{\text{slip}}\\ \omega_{slip} & \frac{L_r}{\sigma L_m^2}R_s\end{bmatrix}\begin{bmatrix}P_s\\ Q_s\end{bmatrix}\\ &\quad - \frac{3}{2}\frac{L_r}{\sigma L_m^2}\begin{bmatrix}u_{s\alpha}^2 + u_{s\beta}^2\\ 0\end{bmatrix},\\ &\quad + \begin{bmatrix}K_P(P_s^* - P_s)\\ K_Q(Q_s^* - Q_s)\end{bmatrix}\end{aligned}$$

and

$$\boldsymbol{D} = \frac{3}{2}\frac{1}{\sigma L_m}\begin{bmatrix}u_{s\alpha} & u_{s\beta}\\ u_{s\beta} & -u_{s\alpha}\end{bmatrix}.$$

In SMC, a Lyapunov approach is used for deriving conditions on the control law that will drive the state orbit to the equilibrium manifold. The quadratic Lyapunov function is selected as

$$W = \frac{1}{2}\boldsymbol{S}^T\boldsymbol{S} \geq 0. \tag{21}$$

The time derivative of W on the state trajectories of (20) is given by

$$\frac{dW}{dt} = \frac{1}{2}\left(\boldsymbol{S}^T\frac{d\boldsymbol{S}}{dt} + \boldsymbol{S}\frac{d\boldsymbol{S}^T}{dt}\right) = \boldsymbol{S}^T\frac{d\boldsymbol{S}}{dt} = \boldsymbol{S}^T(\boldsymbol{F} + \boldsymbol{D}\boldsymbol{U}_{r\alpha\beta}^{s}). \tag{22}$$

The switch control law must be chosen so that the time derivative of W is definitely negative with $\boldsymbol{S} \neq 0$. Thus, the following control law is selected:

$$\boldsymbol{U}_{r\alpha\beta}^{s} = -\boldsymbol{D}^{-1}\left\{\begin{bmatrix}F_1\\F_2\end{bmatrix} + \begin{bmatrix}K_{P1} & 0\\ 0 & K_{Q1}\end{bmatrix}\begin{bmatrix}sgn(S_1)\\ sgn(S_2)\end{bmatrix}\right\} \tag{23}$$

where K_{P1} and K_{Q1} are positive control gains, $sgn(S_1)$ and $sgn(S_2)$ are respective switch functions for active and reactive powers.

3) Proof of the Stability: For stability to the sliding surfaces, it is sufficient to have $dW/dt < 0$. By setting appropriate switch functions, the stability can be achieved provided the following condition is satisfied:

If $S_1 sgn(S_1) > 0$ and $S_2 sgn(S_2) > 0$ then

$$\frac{dW}{dt} = \boldsymbol{S}^T\frac{d\boldsymbol{S}}{dt} = -\boldsymbol{S}^T\begin{bmatrix}K_{P1} & 0\\ 0 & K_{Q1}\end{bmatrix}\begin{bmatrix}sgn(S_1)\\ sgn(S_2)\end{bmatrix}. \tag{24}$$

The time derivative of Lyapunov function dW/dt is definitely negative so that the control system becomes asymptotically stable.

4) Proof of the Robustness: In the practical operation, the sliding surface $\boldsymbol{S}$ will be affected by the parameter variations, AD sample errors, measurement noises, and so on. Thus, (20) should be rearranged as

$$\frac{d\boldsymbol{S}}{dt} = \boldsymbol{F} + \boldsymbol{D}\boldsymbol{U}_{r\alpha\beta}^{s} + \boldsymbol{H} \tag{25}$$

where $\boldsymbol{H} = [H_1 \quad H_2]^T$ represent system disturbances.

Thus, (24) can be rewritten as

$$\frac{dW}{dt} = \boldsymbol{S}^T\frac{d\boldsymbol{S}}{dt} = \boldsymbol{S}^T\left\{\begin{bmatrix}H_1\\H_2\end{bmatrix} - \begin{bmatrix}K_{P1} & 0\\ 0 & K_{Q1}\end{bmatrix}\begin{bmatrix}sgn(S_1)\\ sgn(S_2)\end{bmatrix}\right\}. \tag{26}$$

It is worth noting that if the positive control gains fulfill the following condition, namely, $K_{P1} > |H_1|$ and $K_{Q1} > |H_2|$, the time derivative of Lyapunov function dW/dt is still definitely negative. Thus, the SMC features strong robustness.

5) Remedy of Power Chattering Problem: The SMC scheme developed earlier guarantees the fast tracking of the instantaneous active and reactive powers from DFIG stator side. However, fast switching may generate unexpected chattering, which may excite unmodeled high-frequency system transients and even result in unforeseen instability. To eliminate this problem, the discontinuous part of the controller is smoothed out by introducing a boundary layer around the sliding surface. As a result, a continuous function around the sliding surface neighborhood is obtained as

$$sgn(S_j) = \begin{cases}1, & \text{if } S_j > \lambda_j\\ \dfrac{S_j}{\lambda_j}, & \text{if } |S_j| \leq \lambda_j\\ -1, & \text{if } S_j < -\lambda_j.\end{cases} \tag{27}$$

where $\lambda_j > 0$ is the width of the boundary layer and $j = 1, 2$.

According to (23) and (27), the required control voltage for rotor side converter is obtained in the stator stationary reference frame and can be transformed into rotor reference frame rotating at the angular speed of ω_r as

$$\boldsymbol{U}_{r\alpha\beta}^{r} = \boldsymbol{U}_{r\alpha\beta}^{s}e^{-j\theta_r}. \tag{28}$$

Thus, SVM module is used to generate the required switching voltage vectors and their respective duration times.

6) System Implementation: Fig. 4 shows the schematic diagram of the proposed DPC strategy, using the SMC approach. As shown, the developed SMC directly generates the voltage

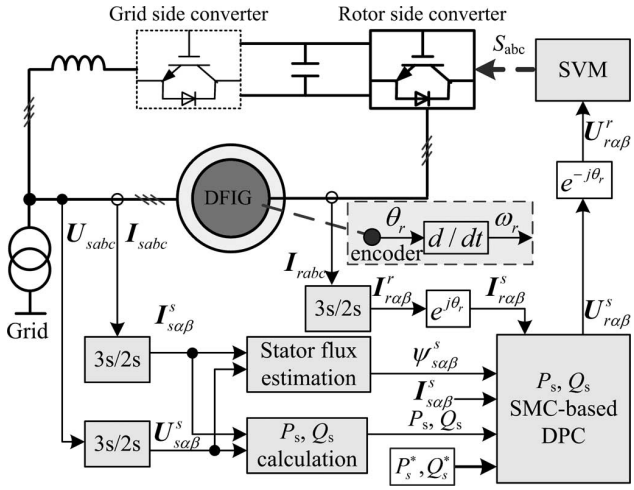

Fig. 4. Schematic diagram of the proposed SMC-based DPC for a grid-connected DFIG.

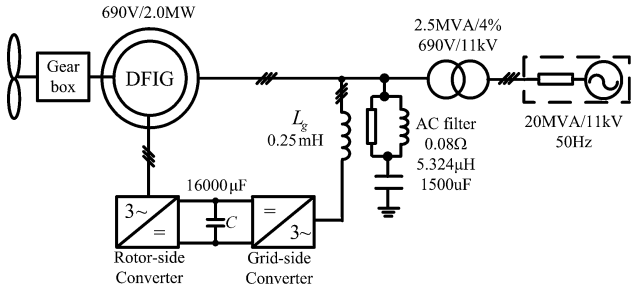

Fig. 5. Scheme of the simulated system.

reference for rotor side converter in the stator stationary reference frame according to the instantaneous errors of active and reactive powers. Afterward, it is transformed into rotor reference frame. Since the maximum output voltage from a converter is limited by its dc-link voltage. During transient conditions, large variations of active and/or reactive power references can result in large power errors within one sampling period. As a result, the required converter's voltage calculated from (23) may exceed the voltage capability of the converter. Thus, $\boldsymbol{U}^r_{r\alpha\beta}$ must be limited properly to improve the transient response. It is worth noting that the control strategy does not require any synchronous coordinate transformations and angular information of network voltage.

IV. Simulation Results

Simulations of the proposed control strategy for a DFIG-based wind power generation system were carried out, using MATLAB/Simulink, and Fig. 5 shows the scheme of the implemented system. Discrete models were used with a simulation time step of 5 μs. The DFIG is rated at 2 MW with its parameters given in Table I. The nominal converter dc-link voltage was set at 1200 V. The grid side converter has to maintain a constant dc-link voltage, and it is controlled by a method similar to the dc voltage controller in a PWM voltage source rectifier [28], which is not included here. During simulations, a sampling frequency of 4 kHz was used for the proposed control strategy. Due to the use of an asymmetric SVM technique, a 1-kHz converter switching frequency was set. As shown in Fig. 5, a high-frequency ac filter is connected to the stator side to absorb the switching harmonics generated by the two converters. The filter is a single-tuned filter with inductance and resistance connected in parallel instead of series, which results in a wideband filter having an impedance at high frequencies limited by the resistance [29].

TABLE I
Parameters of the Simulated DFIG System

Rated power	2.0MW
Line-to-line voltage (rms)	690 V
Stator frequency	50Hz
Stator-to-rotor ratio	3
R_s (ohm)	0.001518
R_r (ohm) (referred to the stator)	0.002087
$L_{\sigma s}$ (mH)	0.059906
$L_{\sigma r}$ (mH) (referred to the stator)	0.082060
L_m (mH)	2.4
Pole pairs	2
Lumped inertia constant (kg·m^2)	17.23

TABLE II
Control Parameters of SMC Regulator

Positive gains K_P and K_Q	3500
Control gains K_{P1} and K_{Q1}	35000
Width of boundary layer λ_1, λ_2	200000, 250000

In a practical system, voltages and currents are sampled at the beginning of each sampling period. The required rotor control voltage for the sampling period is, then, calculated and passed to the SVM module. Inevitably, there is a time delay between the instant sampling and SVM modulator's receiving the required rotor control voltage and updating its register values. Rotor voltage calculation of the proposed DPC strategy is relatively simple, and the time delay should be pretty small. Nevertheless, the calculated output rotor voltage is delayed by 250 μs (one sampling period) to closely represent a practical DPC control system. During the simulation, the grid side converter is enabled first, so that the converter dc-link voltage is regulated. The generator is, then, excited by rotor-side converter with the rotor rotating at a fixed speed till the stator voltage matches with the network voltage, such that the DFIG system is switched into grid-connected operation. This starting process is not shown in the following results.

A. Comparative Studies

In order to verify the performance of the proposed DPC strategy based on SMC approach, comparative simulations involving classic voltage-oriented VC, conventional LUT DPC, and SMC DPC were initially conducted with rotor speed of 1.2 pu (supersynchronous speed, 1800 r/min). The PI parameters of the VC current controller were 0.12 and 0.005 s, respectively. For the LUT DPC, the sampling time was set at 20 kHz [13], and the bandwidths of the active and reactive power hysteresis controllers were set at $\pm 2\%$ of the rated generator power of 2 MW. While for the proposed SMC DPC approach, the control parameters are listed in Table II.

Fig. 6(A)–(C) compares the system response during various active and reactive power steps for the conventional LUT DPC, proposed SMC DPC, and VC, respectively. As shown in Fig. 6,

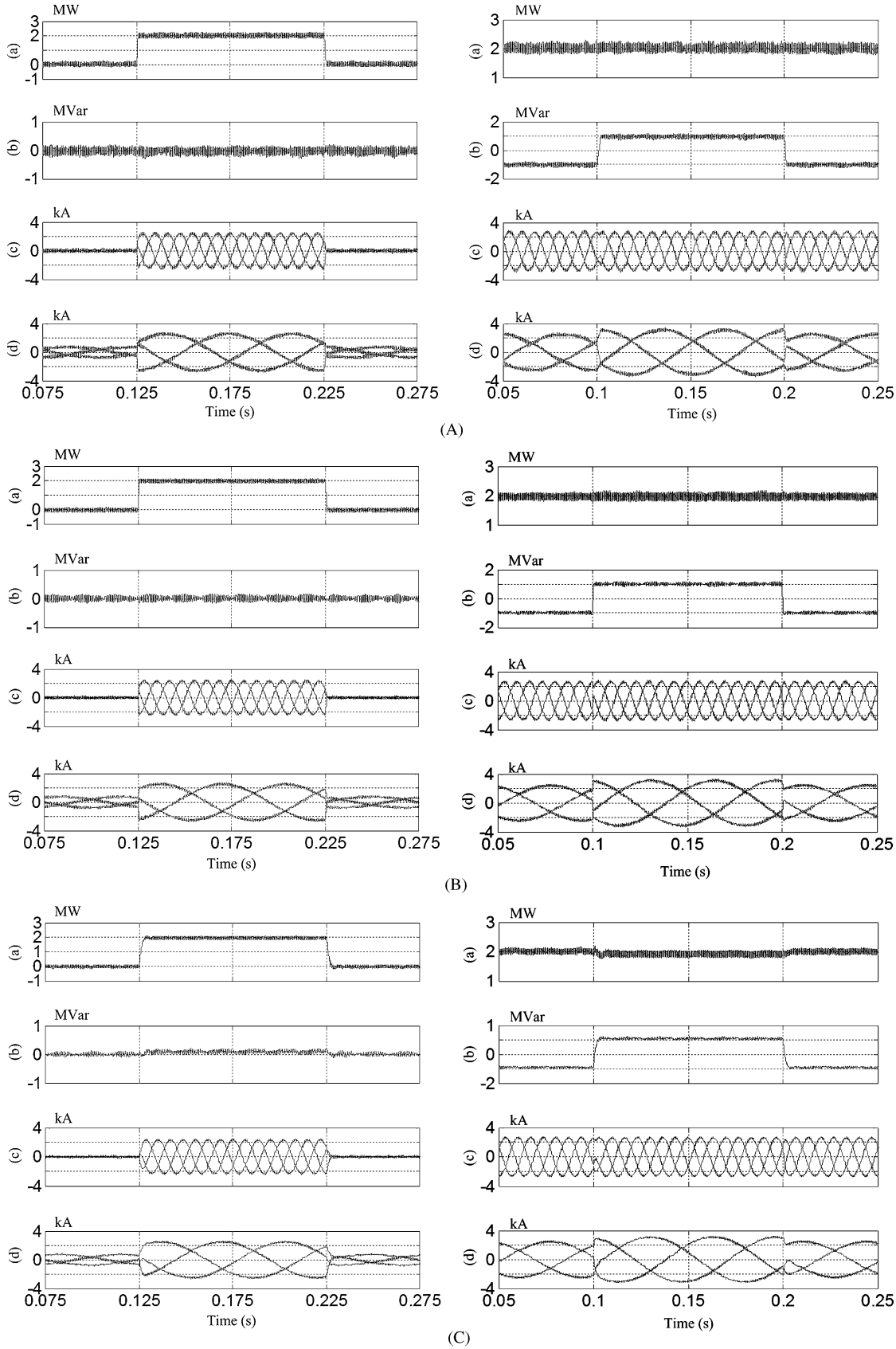

Fig. 6. Simulation results using three different control strategies during various stator active and reactive power steps. (a) Active power output (MW). (b) Reactive power output (MVar). (c) Three-phase stator currents (kA). (d) Three-phase rotor currents (kA). (A) Conventional LUT DPC. (B) Proposed SMC DPC. (C) Classic VC.

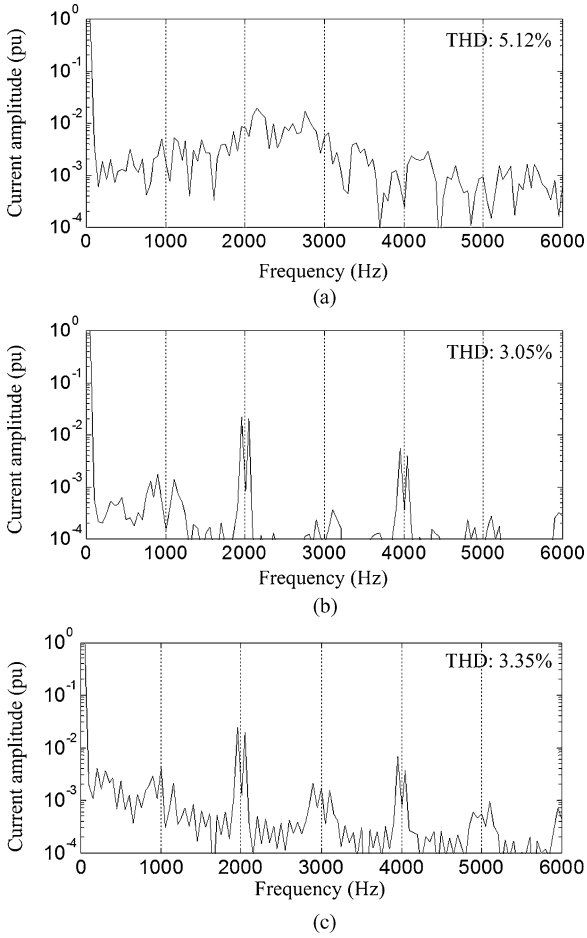

Fig. 7. Stator current harmonic spectra: $P_s = 2$ MW, $Q_s = 1$ MVar. (a) Conventional LUT DPC. (b) Proposed SMC DPC: switching frequency $= 1$ kHz. (c) Classic VC: switching frequency $= 1$ kHz.

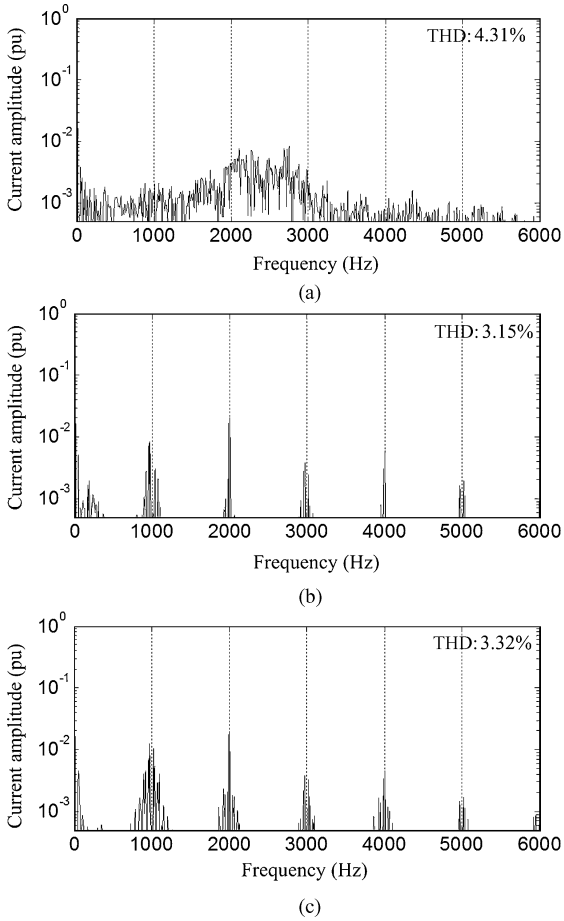

Fig. 8. Rotor current harmonic spectra: $P_s = 2$ MW, $Q_s = 1$ MVar. (a) Conventional LUT DPC. (b) Proposed SMC DPC: switching frequency $=$ 1 kHz. (c) Classic VC: switching frequency $= 1$ kHz.

the active power is stepped from 0 to 2 MW (export of active power from the DFIG to grid) at 0.125 s and then backed to 0 at 0.225 s, while the reactive power is stepped from -1 (inductive) to 1 MVar (capacitive) at 0.1 s and backed to -1 MVar at 0.2 s. The transient responses of both active and reactive powers for the two DPC strategies are within a few milliseconds, whereas the dynamic response of the VC is largely determined by the PI parameters of the current controller. It is clearly seen that for the proposed SMC DPC strategy, the step change of one control variable, i.e., stator active or reactive power, does not affect the other, and there is no overshoot of either the stator and rotor currents or the active and reactive powers.

To further compare the performance of three control methods, Figs. 7 and 8, respectively give the stator and rotor current harmonic spectra with $P_s = 2$ MW and $Q_s = 1$ MVar for different control strategies. Obviously, conventional LUT DPC results in higher stator current harmonic distortion than those from SMC DPC and classic VC. Besides, the LUT DPC results in broadband harmonic spectra, whereas SMC DPC produces similar deterministic harmonics as VC with dominant harmonics around the 1 kHz switching frequency and multiples thereof. Thus, it can be concluded from the results that the proposed SMC-based DPC proives enhanced transient performance sililar to the LUT

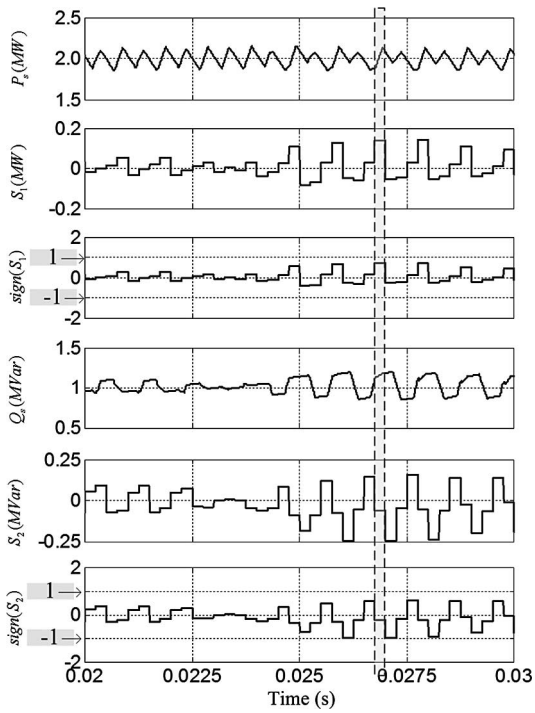

Fig. 9. Active and reactive power errors and associated switch functions.

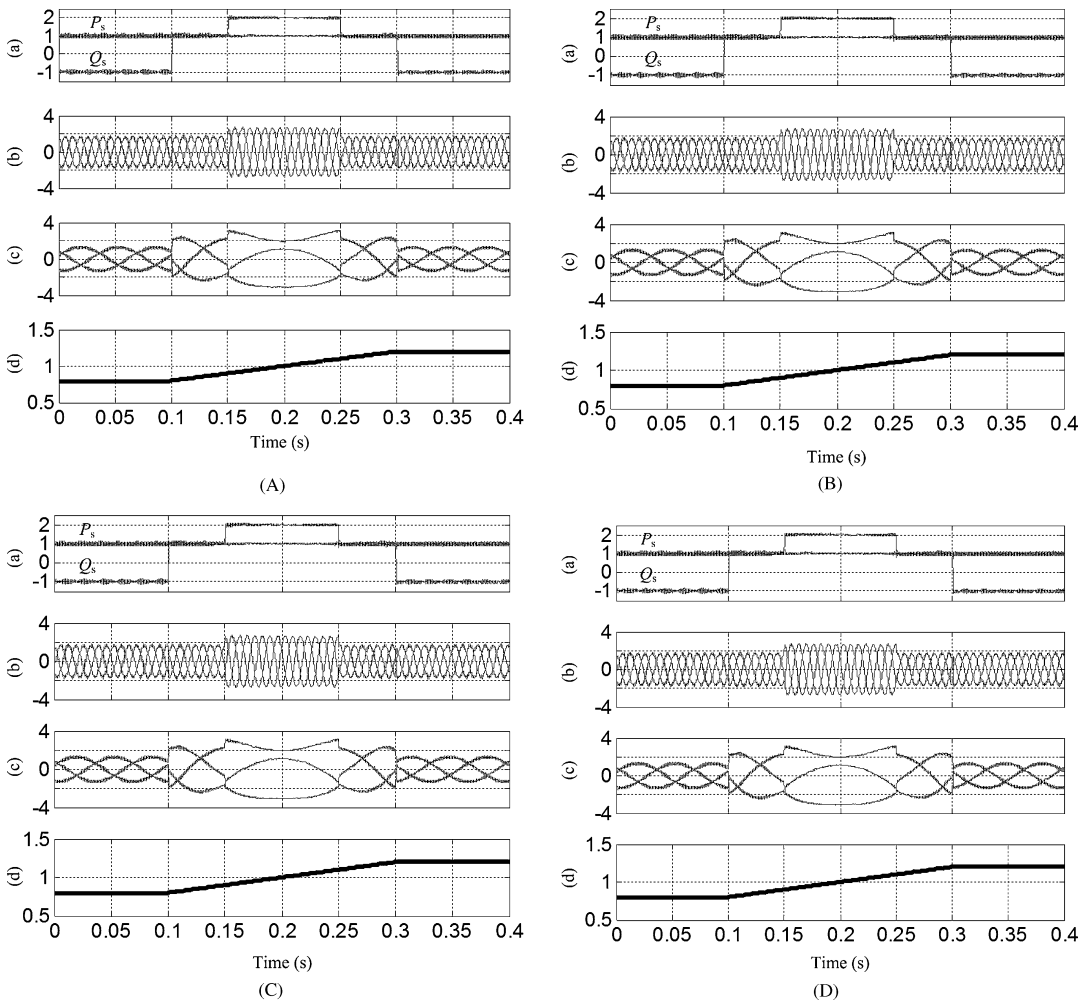

Fig. 10. Simulated results under various stator active and reactive power steps and rotor speed variations. (a) Stator active power (MW) and reactive power (MVar). (b) Three-phase stator currents (kA). (c) Three-phase rotor currents (kA). (d) Rotor speed (pu). (A) With no L_m, R_s, R_r errors. (B) With -50% L_m, -50% R_s, -50% R_r errors. (C) With $+50\%$ L_m, -50% R_s, -50% R_r errors. (D) With $+50\%$ L_m, $+50\%$ R_s, $+50\%$ R_r errors.

DPC, and meanwhile keeps the steady-state harmonic spectra at the same level as the classic VC due to the use of SVM modulation technique, as shown in Fig. 4. For different operation conditions, such as different active/reactive powers and rotor speeds, the system reponses and stator current harmonic spectra behave similarly to those shown in Figs. 6, 7 and 8.

B. *Effect of Switch Functions $sgn(S_1)$ and $sgn(S_2)$*

In order to confirm the effectiveness of the remedy for power chattering problems with the proposed SMC DPC strategy, Fig. 9 shows the active and reactive power errors and associated continuous switch functions. Taking the shadow in Fig. 9 as an example, during the sampling period the active power error is within the width of the positive boundary layer, namely, $0 < S_1 < 200\,000$, thus the active power switch function $sgn(S_1)$ is $0 < S_1/\lambda_1 < 1$. Meanwhile for the reactive power, the error is within the width of the negative boundary layer, which is $-250\,000 < S_2 < 0$, as a result, the reactive power switch function $sgn(S_2)$ is set at $-1 < S_2/\lambda_2 < 0$. The switch functions during other sampling periods are similar, which is not explained thoroughly here due to space limitation.

C. *Robustness to Parameters Mismatch*

Further tests of the impact of DFIG's parameters variations on both steady state and transient performance with SMC DPC were carried out. Since the leakage flux magnetic path is mainly air in the generator, the variations of the stator and rotor leakage inductances during operation are insignificant. However, mutual inductance variation needs to be considered due to possible variation of the magnetic permeability of the stator and rotor cores under different operating conditions. Besides, variations of stator and rotor resistances should also be taken into account. Fig. 10(A)–(D) shows the simulation results with mutual inductance and stator and rotor resistances used in the controller having various errors, respectively. As shown, during the period of 0.1–0.3 s, the rotor speed increased from 0.8 pu (subsynchronous speed, 1200 r/min) to 1.2 pu. Various stator power steps were applied, namely, active power references were changed from 1 to 2 MW at 0.15 s and backed to 1 MW at 0.25 s and, meanwhile, the reactive power references changed from -1 (inductive) to 1 MVar (capacitive) at 0.1 s and backed to -1 MVar at 0.3 s. As shown in Fig. 10(A), the system response with rotor speed variations is satisfactory. Comparing Fig. 10(A)–(D), there are

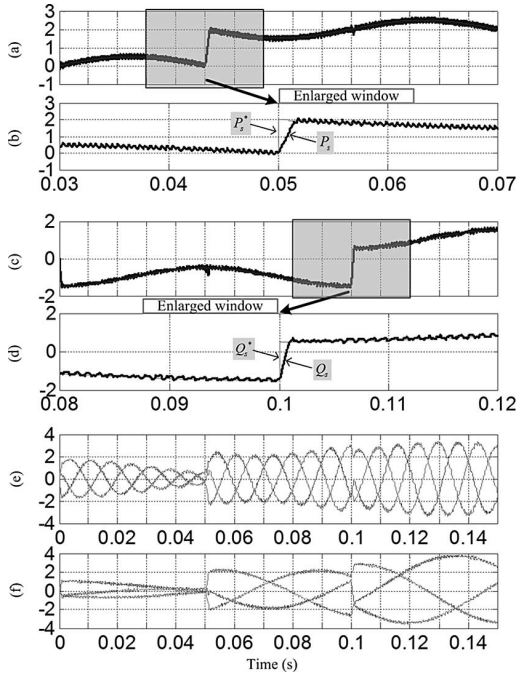

Fig. 11. Tracking behavior of the proposed SMC DPC with stator active and reactive powers sinusoidally varying and step changes. (a) Stator active power (MW). (b) Stator active power (MW) (enlarged window between 0.03 and 0.07 s). (c) Stator reactive power (MVar). (d) Stator reactive power (MVar) (enlarged window between 0.08 and 0.12 s). (e) Three-phase stator currents (kA). (f) Three-phase rotor currents (kA).

hardly any differences even with such large errors in the mutual inductance and stator and rotor resistances. The generation system retains pretty good performance under both steady state and transient conditions. As a result, robustness of the proposed SMC DPC to generator parameters' variations is verified.

D. Tracking Behavior

In the wind power generation system, the DFIG is required to operate at variable speed and, meanwhile, the required active and reactive power references may also be variable. Under this circumstance, the adopted control strategy should guarantee that the actual values should track their references as closely as possible. Thus, it is important to demonstrate the SMC DPCs precise tracking capability with high-control bandwidth. Fig. 11 shows the study result, where a sinusoidally varying reference with amplitude of 0.25 pu and frequency of 10 Hz is imposed to the average stator active and reactive power references, respectively. The average stator active and reactive power demands were step changed from 0 to 2 MW at 0.05 s and from -1 to 1 MVar at 0.1 s, respectively. As can be seen, the proposed SMC-DPC strategy is capable of providing accurate tracking for both active and reactive powers even with time-varying demanded references.

E. Response of MPPT

Further tests for an entire wind power generation system composed of a typical 2-MW wind turbine and the DFIG were carried out. The DFIG was set in torque control, i.e., the speed is the result of stator–rotor voltage–current and the mechanical torque. The active power reference for the DFIG was calculated from the maximum power-tracking curve [22]. Fig. 12 shows the simulated results when the wind speed changed from 8 to 12.5 m/s at 1.5 s, and then to 9 m/s at 2.5 s. Meanwhile, the stator reactive power was step changed from -1 to 1 MVar at 2 s and backed to 0 Var at 3 s. The lumped inertia constant of the system is set to a relatively small value of $17.23kg{\cdot}m^2$ in the study to reduce the simulation time. As can be seen from Fig. 12, the system operation is satisfactory and maximum power tracking is achieved when wind speed varies.

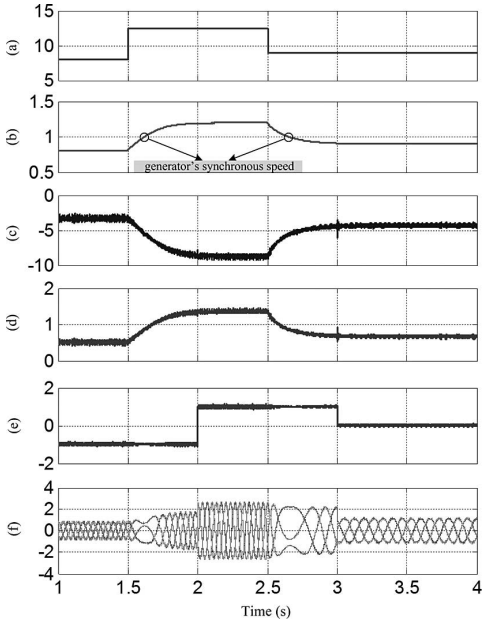

Fig. 12. Simulated results of an entire DFIG-based wind generation system with step change of wind speed. (a) Wind speed (m/s). (b) Generator speed (pu). (c) Electromagnetic torque (kNm). (d) Stator active power (MW). (e) Stator reactive power (MVar). (f) Three-phase rotor currents (kA).

V. Conclusion

This paper has proposed a new DPC for grid connected DFIG systems based on SMC approach. Simulation results on a 2-MW grid-connected DFIG system have been provided and compared with those of classic VC and conventional LUT DPC. The main features of the proposed SMC-based DPC strategy are as follows.

1) No synchronous coordinate transformations and angular information of grid voltage or stator flux are required.
2) Enhanced transient performance similar to the conventional LUT DPC is obtained.
3) Steady-state stator and rotor current harmonic spectra are kept at the same level as the classic VC strategy due to the use of SVM modulation technique.
4) The steady state and transient responses are insensitive to the machine parameters' variations.

Acknowledgment

The authors would like to thank the reviewers and the editor for their valuable comments and suggestions that helped in improving this paper.

REFERENCES

[1] S. Muller, M. Deicke, and R. W. De Doncker, "Doubly fed induction generator systems for wind turbines," *IEEE Ind. Appl. Mag.*, vol. 8, no. 3, pp. 26–33, May/Jun. 2002.

[2] J. Hu, Y. He, L. Xu, and B. W. Williams, "Improved control of DFIG systems during network unbalance using PI-R current regulators," *IEEE Trans. Ind. Electron.*, vol. 56, no. 2, pp. 439–451, Feb. 2009.

[3] R. Pena, J. C. Clare, and G. M. Asher, "Doubly fed induction generator using back-to-back PWM converter and is application to variable-speed wind–energy generation," *Proc. IEE B Electr. Power Appl.*, vol. 143, no. 3, pp. 231–241, May 1996.

[4] J. Hu and Y. He, "Dynamic modeling and robust current control of wind-turbine used DFIG during AC voltage dip," *J. Zhejiang Univ. Sci. A*, vol. 7, no. 10, pp. 1757–1764, Oct. 2006.

[5] I. Takahashi and T. Noguchi, "A new quick-response and high-efficiency control strategy of an induction motor," *IEEE Trans. Ind. Appl.*, vol. IA-22, no. 5, pp. 820–827, Sep. 1986.

[6] M. Depenbrock, "Direct self-control (DSC) of inverter-fed induction machine," *IEEE Trans. Power Electron.*, vol. PEL-3, no. 4, pp. 420–429, Oct. 1988.

[7] G. S. Buja and M. P. Kazmierkowski, "Direct torque control of PWM inverter-fed ac motors-a survey," *IEEE Trans. Ind. Electron.*, vol. 51, no. 4, pp. 744–575, Aug. 2004.

[8] Y. S. Lai and J. H. Chen, "A new approach to direct torque control of induction motor drives for constant inverter switching frequency and torque ripple reduction," *IEEE Trans. Energy Convers.*, vol. 16, no. 3, pp. 220–227, Sep. 2001.

[9] N. R. N. Idris and A. H. M. Yatim, "Direct torque control induction machines with constant switching frequency and reduced torque ripple," *IEEE Trans. Ind. Electron.*, vol. 51, no. 4, pp. 758–767, Aug. 2004.

[10] T.G. Habetler, F. Profumo, M. Pastorelli, and L.M. Tolbert, "Direct torque control of induction machines using space vector modulation," *IEEE Trans. Ind. Appl.*, vol. 28, no. 5, pp. 1045–1053, Sep. 1992.

[11] J. Kang and S. Sul, "New direct torque control of induction motor for minimum torque Ripple and constant switching frequency," *IEEE Trans. Ind. Appl.*, vol. 35, no. 5, pp. 1076–1082, Sep./Oct. 1999.

[12] R. Datta and V. T. Ranganathan, "Direct power control of grid-connected wound rotor induction machine without rotor position sensors," *IEEE Trans. Power Electron.*, vol. 16, no. 3, pp. 390–399, May 2001.

[13] L. Xu and P. Cartwright, "Direct active and reactive power control of DFIG for wind energy generation," *IEEE Trans. Energy Convers.*, vol. 21, no. 3, pp. 750–758, Sep. 2006.

[14] G. Abad, M. A. Rodriguez, and J. Poza, "Two-level VSC-based predictive direct power control of the doubly fed induction machine with reduced power ripple at low constant switching frequency," *IEEE Trans. Energy Convers.*, vol. 23, no. 2, pp. 570–580, Jun. 2008.

[15] G. Abad, M. A. Rodriguez, and J. Poza, "Two-level VSC-based predictive torque control of the doubly Fed induction machine with reduced torque and flux ripples at low constant switching frequency," *IEEE Trans. Power Electron.*, vol. 23, no. 3, pp. 1050–1061, May 2008.

[16] D. Zhi and L. Xu, "Direct power control of DFIG with constant switching frequency and improved transient performance," *IEEE Trans. Energy Convers.*, vol. 22, no. 1, pp. 110–118, Mar. 2007.

[17] J. Hu, Y. He, and L. Xu, "Dynamic modeling and direct power control of wind turbine driven DFIG under unbalanced network voltage conditions," *J. Zhejiang Univ. Sci. A*, vol. 9, no. 12, pp. 1731–1740, Dec. 2008.

[18] V. I. Utkin, "Sliding mode control design principles and applications to electric drives," *IEEE Trans. Ind. Electron.*, vol. 40, no. 1, pp. 23–36, Feb. 1993.

[19] C. Lascu, I. Boldea, and F. Blaabjerg, "Direct torque control of sensorless induction motor drives: a sliding-mode approach," *IEEE Trans. Ind. Appl.*, vol. 40, no. 2, pp. 582–590, Mar./Apr. 2004.

[20] C. Lascu, I. Boldea, and F. Blaabjerg, "Very-low-speed variable-structure control of sensorless induction machine drives without signal injection," *IEEE Trans. Ind. Appl.*, vol. 41, no. 2, pp. 591–598, Mar./Apr. 2005.

[21] B. Beltran, T. Ahmed-Ali, and M. E. H. Benbouzid, "Sliding mode power control of variable-speed wind energy conversion systems," *IEEE Trans. Energy Convers.*, vol. 23, no. 2, pp. 551–558, Jun. 2008.

[22] B. Beltran, T. Ahmed-Ali, and M. E. H. Benbouzid, "High-order sliding-mode control of variable-speed wind turbines," *IEEE Trans. Ind. Electron.*, vol. 56, no. 9, pp. 3314–3321, Sep. 2009.

[23] S. E. Ben Elghali, M. E. H. Benbouzid, T. Ahmed-Ali, J. F. Charpentier, and F. Mekri, "High-order sliding mode control of DFIG-based marine current turbine," in *Proc. IEEE IECON 2008*, Orlando, FL, Nov, pp. 1228–1233.

[24] B. Beltran, T. Ahmed-Ali, and M. E. H. Benbouzid, "High-order sliding mode control of a DFIG-based wind turbine for power maximization and grid fault tolerance," in *Proc. IEEE IEMDC 2009*, Miami, FL, May, pp. 183–189.

[25] M. Bouri and D. Thomasset, "Sliding control of an electropneumatic actuator using an integral switching surface," *IEEE Trans. Control Syst. Technol.*, vol. 9, no. 2, pp. 368–374, Mar. 2001.

[26] S. K. Chung, J. H. Lee, J. S. Ko, and M. J. Youn, "Robust speed control of brushless direct-drive motor using integral variable structure control," *Proc. IEE B Electr. Power Appl.*, vol. 142, no. 6, pp. 361–370, May 1996.

[27] Z. Xu and M. F. Rahman, "Direct torque and flux regulation of an IPM synchronous motor drive using variable structure control approach," in *Proc. 30th Annu. Conf. IEEE (IECON 2004)*, Nov. 2–6, pp. 2733–2738.

[28] V. Pedro and G. D. Marques, "DC voltage control and stability analysis of PWM-voltage-type reversible rectifier," *IEEE Trans. Ind. Electron.*, vol. 45, no. 2, pp. 263–273, Apr. 1998.

[29] F. Peng, H. Akagi, and A. Nabe, "A new approach to harmonic compensation in power systems – a combined system of shunt passive and series active filters," *IEEE Trans. Ind. Appl.*, vol. 26, no. 6, pp. 983–990, Nov./Dec. 1990.

Jiabing Hu (S'05–M'10) received the B.Sc. and Ph.D. degrees from the College of Electrical Engineering, Zhejiang University, Hangzhou, China, in 2004 and 2009, respectively.

He is currently a Research Associate at the Department of Electronic and Electrical Engineering, University of Sheffield, Sheffield, U.K. From 2007 to 2008, he was as a Visiting Scholar at the Department of Electronic and Electrical Engineering, University of Strathclyde, Glasgow, U.K. His research interests include motor drives and the application of power electronics in renewable energy conversion, especially the control and operation of doubly fed induction generator and permanent magnet synchronous generator for wind power generation.

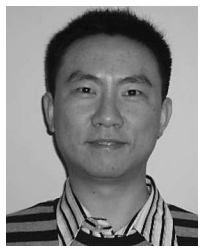

Heng Nian (M'09) received the B.Eng. and M.Eng. degrees from Hefei University of Technology, Hefei, China, in 1999 and 2002, and the Ph.D. degree from Zhejiang University, Hangzhou, China, in 2005, all in electrical engineering.

From 2005 to 2007, he was as a Postdoctoral Researcher at the College of Electrical Engineering, Zhejiang University, China, where he has been an Associate Professor at the College of Electrical Engineering, Zhejiang University since 2007. His current research interests include the optimal design and operation control for wind power generation system.

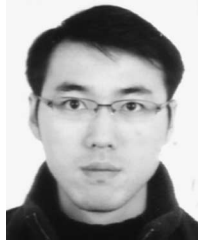

Bin Hu was born in Hangzhou, Zhejiang, China, in 1981. He graduated with Dipl.-Ing. degree from the Institutes of Electrical Engineering, University Stuttgart, Stuttgart, Germany, in 2007, and the Bachelor's degree from the College of Electrical Engineering, Zhejiang University, Hangzhou, China, in 2003.

Since August 2007, he has been with Zhejiang Wind Power Development Corporation Ltd., Hangzhou, China. His current research interests include electric power system of wind park, and application of power electronics in renewable energy conversion.

Yikang He (SM'90) was born in Changsha, Hunan, China. He graduated from the Department of Electrical Engineering, Tsinghua University, Beijing, China, in 1964.

Since 1964, he has been a Teacher at the College of Electrical Engineering, Zhejiang University, Hangzhou, China, where he is currently a Professor. His research interests include electric machinery, motor control, power electronics, and renewable energy conversion.

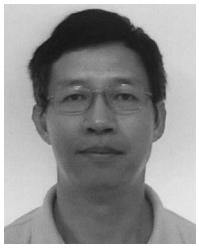

Z. Q. Zhu (M'90–SM'00–F'09) received the B.Eng. and M.Sc. degrees in electrical and electronic engineering from Zhejiang University, Hangzhou, China, in 1982 and 1984, respectively, and the Ph.D. degree in electronic and electrical engineering from The University of Sheffield, Sheffield, U.K., in 1991.

From 1984 to 1988, he was a Lecturer in the Department of Electrical Engineering, Zhejiang University. Since 1988, he has been with The University of Sheffield, where he was initially a Research Associate and was subsequently appointed to an established post as Senior Research Officer/Senior Research Scientist. Since 2000, he has been a Professor of electrical machines and control systems in the Department of Electronic and Electrical Engineering, The University of Sheffield, and is currently Head of the Electrical Machines and Drives Research Group. His current major research interests include design and control of permanent-magnet brushless machines and drives, for applications ranging from automotive and aerospace to renewable energy.